

高压物理学报

陶瓷材料宏观动态新本构模型

唐瑞涛 徐柳云 文鹤鸣 王子豪

A Macroscopic Dynamic Constitutive Model for Ceramic Materials

TANG Ruitao, XU Liyun, WEN Heming, WANG Zihao

引用本文:

唐瑞涛, 徐柳云, 文鹤鸣, 等. 陶瓷材料宏观动态新本构模型[J]. 高压物理学报, 2020, 34(4):044201. DOI: 10.11858/gywlb.20190863

TANG Ruitao, XU Liyun, WEN Heming, et al. A Macroscopic Dynamic Constitutive Model for Ceramic Materials[J]. Chinese Journal of High Pressure Physics, 2020, 34(4):044201. DOI: 10.11858/gywlb.20190863

在线阅读 View online: <https://doi.org/10.11858/gywlb.20190863>

您可能感兴趣的其他文章

Articles you may be interested in

正交各向异性材料的三维动态本构模型及其在脉冲X射线热击波模拟中的应用

A Dynamic Constitutive Model of Anisotropic Material in Three-Dimensional Strain and Its Application in the Simulation of Thermal Shock Wave Induced by X-Ray Radiation

高压物理学报. 2017, 31(6): 727 <https://doi.org/10.11858/gywlb.2017.06.007>

简论金属材料JC本构模型的精确性

On the Accuracy of the Johnson-Cook Constitutive Model for Metals

高压物理学报. 2019, 33(4): 042101 <https://doi.org/10.11858/gywlb.20190721>

5083铝合金宽应变率实验与基于损伤的本构模型研究

Experimental Study of Wide Strain Rates and Constitutive Model Based on Damage of 5083 Aluminum Alloy

高压物理学报. 2017, 31(1): 51 <https://doi.org/10.11858/gywlb.2017.01.008>

考虑温度效应的泡沫铝准静态压缩本构模型

Constitutive Model of Aluminum Foams Considering Temperature Effect under Quasi-Static Compression

高压物理学报. 2018, 32(4): 044103 <https://doi.org/10.11858/gywlb.20170642>

比较93钨合金材料的3种本构模型

Comparative Analysis of 3 Constitutive Models for 93 Tungsten Alloy

高压物理学报. 2017, 31(6): 753 <https://doi.org/10.11858/gywlb.2017.06.010>

金属材料失效分析的新方法

A New Approach for the Failure of Metallic Materials

高压物理学报. 2019, 33(1): 014103 <https://doi.org/10.11858/gywlb.20180613>

DOI: 10.11858/gywlxb.20190863

A Macroscopic Dynamic Constitutive Model for Ceramic Materials

TANG Ruitao, XU Liyun, WEN Heming, WANG Zihao

(CAS Key Laboratory for Mechanical Behavior and Design of Materials,
University of Science and Technology of China, Hefei 230027, Anhui, China)

Abstract: A macroscopic constitutive model is presented herein for ceramic materials subjected to dynamic loadings by closely following a previous study on concrete. The equation of state is described by a polynomial equation and the strength model takes into account various effects such as pressure hardening, Lode angle, strain rate, shear damage and tensile softening. In particular, the strength surface of ceramic materials is characterized by a new function which levels out at very high pressures and strain rate effect is taken into account by dynamic increase factor (DIF) which excludes inertial effect. The present model is verified against some available experimental data for ceramic materials in terms of pressure-volumetric response, quasi-static strength surface and strain rate effect. The model is further verified against the data for triaxial test by single element simulation approach and the test data for depth of penetration in AD99.5/RHA struck by tungsten alloy penetrators. Furthermore, comparisons are also made between numerical results of the present model and the JH-2 model. It is demonstrated that the present model can be employed to describe the mechanical behavior of ceramic materials under different loading conditions with reasonable confidence and is advantageous over the existing model.

Keywords: ceramic material; constitutive model; strain rate effect; triaxial test; JH-2 model; single element simulation approach

CLC number: O347.3

Document code: A

Ceramic materials have been increasingly used in armors, personal armor system, aeronautic engineering and vehicle engineering due to its excellent ballistic performance. An understanding of the response and failure of ceramic materials under impact loading is of great significance for the design and assessment of military hardware and protective structures.

As ballistic tests are expensive to perform and time consuming, numerical simulations have been widely employed in the design and optimization of ceramic armors. However, the accuracy of numerical simulations depends on the dynamic constitutive model for ceramic materials to a large extent. To this end, many models have been put forward^[1-8]. Fahrenthold^[1] proposed a continuum damage model for fracture of brittle solids under dynamic loading in which Weibull strength distribution was employed to account for the effects of flaw size distribution on the damage accumulation rate. The model was used to compute the depth of penetration in a steel plate impacted by a sphere of alumina without being applied to simulate the behavior of ceramic armors subjected

* **Received date:** 2019-12-06; **Revised date:** 2020-01-06

Biography: TANG Ruitao (1989—), male, doctoral student, major in impact dynamics.

E-mail: rttang@mail.ustc.edu.cn

Corresponding author: WEN Heming (1965—), male, Ph.D, professor, major in impact dynamics.

E-mail: hmwen@ustc.edu.cn

to projectile impact. Rajendran^[2] modeled the impact behavior of AD85 ceramic under multiaxial loading by assuming an existing distribution of micro-cracks and employing a criterion for crack growth based on theories of dynamic fracture mechanics. The strength of the intact material was rate dependent, and the inelastic deformation was modeled using an elastic-plastic cracking rule. The model predictions were found to be in good agreement with the test data obtained from plate impact tests. The most widely used constitutive model for ceramic materials in many commercial codes is the Johnson-Holmquist model (JH-2)^[3]. The model employs two strength surfaces to describe the pressure-dependent compressive strength of the intact and failed materials, respectively. However, in the model strain rate effect is described by the same form of function adopted in the constitutive models for metals and concrete materials, which has been found to be inconsistent with the dynamic mechanical behavior in recent studies^[9-12]. Furthermore, tensile softening cannot be accurately predicted, and no differentiation was made between the effects of strain rate and inertia (containment).

The main objective of this paper is to establish a macroscopic dynamic constitutive model for ceramic materials by closely following the previous work on concrete^[9] and on the basis of the experimental observations for some ceramic materials. Various equations of the constitutive model are given and compared with some available experimental data for ceramic materials in terms of pressure-volumetric response, quasi-static strength surface and strain rate effect. Furthermore, the model is also verified against the data for triaxial test by single element simulation approach.

1 A Macroscopic Constitutive Model for Ceramics

A dynamic macroscopic constitutive model for ceramic materials is developed in the following sections based on the computational constitutive model for concrete subjected to dynamic loadings^[9] with some modifications being made. There are two points which should be highlighted here, namely, (1) the pressure-volumetric response is described by polynomial equation and the phase transition (e.g. AlN ceramics) as the pressure increases to a certain value is considered; (2) a hyperbolic tangent function is employed to describe the pressure dependent shear strength surfaces of ceramic materials which level out at very high pressures.

1.1 Equation of State

Ceramics are complex granular materials, which contain a large number of micro cracks and voids just as concrete material. On the one hand, it has been observed experimentally that the volumetric strains of Al₂O₃ and SiC increase with increasing pressure^[13-16] and the equation of state for this category of ceramic materials can be expressed as polynomial equation, viz.

$$\begin{cases} p = K_1\mu + K_2\mu^2 + K_3\mu^3 \\ \mu = V_0/V - 1 = \rho/\rho_0 - 1 \end{cases} \quad (1)$$

where p is pressure; μ is volumetric strain; K_1, K_2, K_3 are bulk moduli for ceramic material; $\rho_0 = 1/V_0$ and $\rho = 1/V$ indicate initial and current densities of ceramic material, respectively. On the other hand, the pressure-volumetric response of AlN has been observed experimentally to be quite different^[17-19] and a phase transformation occurs from wurtzite structure to salt structure as pressure reaches a critical value. Thus, the equation of state for such ceramics as AlN can be written in the following form, namely

$$p = \begin{cases} K_1\mu + K_2\mu^2 + K_3\mu^3 & \mu < \mu_{c1} \\ p_c & \mu_{c1} \leq \mu \leq \mu_{c2} \\ K_4(\mu - \mu') + K_5(\mu - \mu')^2 + K_6(\mu - \mu')^3 & \mu > \mu_{c2} \end{cases} \quad (2)$$

where p_c represents a constant pressure at which phase transformation occurs; K_4, K_5, K_6 are bulk moduli for ceramic material after the phase transformation; μ' is an offset in volumetric strain due to phase transformation; μ_{c1} and μ_{c2} are volumetric strains at the beginning and end of phase transformation, respectively. For $\mu < 0$, ceramic

material is under tension condition. Thus, one obtains

$$p = K_1 \mu \quad (3)$$

1.2 Strength Model

On the basis of the previous studies on concrete^[9-10] and the experimental observations for ceramic materials^[17, 20-24], it is suggested that the strength surface of ceramic materials can be cast into the following form, i.e.

$$Y = \begin{cases} 3(p + f_t) r(\theta, e) & p < 0 \\ [3f_t + (f_{cc} - 3f_t) \times 3p/f_{cc}] r(\theta, e) & 0 \leq p \leq f_c/3 \\ [f_{cc} + Bf'_c \tanh(p/f'_c - f_{cc}/(3f'_c))] r(\theta, e) & p > f_c/3 \end{cases} \quad (4)$$

in which Y is shear strength; $f_{cc} = f'_c \psi_c \eta_c$ and $f_t = f_t \psi_t \eta_t$ are respective dynamic strengths of ceramic materials in uniaxial compression and tension, which take account of shear damage in the form of damage shape functions (η) and strain rate effects by dynamic increase factor (DIF); B is an empirical constant; $r(\theta, e)$ represents Lode effect. The dynamic increase factor in compression (ψ_c) can be obtained by the following equation^[9-10], viz.

$$\psi_c = \frac{f_{cd}}{f'_c} = (\psi_t - 1) \frac{f_t}{f'_c} + 1 \quad (5)$$

where f_{cd} and f'_c are the dynamic and static uniaxial compressive strength, respectively, f_t is the static uniaxial tensile strength, and ψ_t represents the dynamic increase factor in tension which is expressed as follows

$$\psi_t = \frac{f_{td}}{f_t} = \left\{ \left(\frac{F_m}{W_y} - 1 \right) \tanh \left[\left(\lg \frac{\dot{\varepsilon}}{\dot{\varepsilon}_0} - W_x \right) S \right] + 1 \right\} W_y \quad (6)$$

in which f_{td} is the dynamic uniaxial tensile strength, parameters W_x , F_m , W_y and S are constants to be determined experimentally, $\dot{\varepsilon}$ is the strain rate, $\dot{\varepsilon}_0$ is the reference strain rate usually taken to be $\dot{\varepsilon}_0 = 1.0 \text{ s}^{-1}$.

The multi-axial tests of ceramics show that the effective strain at maximum load (ε_{\max}) increases almost linearly with increasing pressure. Furthermore, these tests also show ceramic compressive strength has no significant influence on this behavior. According to Eq.(18) in Ref.[9], the failure strain of ceramic is written as

$$\varepsilon_f = \frac{\varepsilon_m}{\lambda_m} \left(\frac{\dot{\varepsilon}}{\dot{\varepsilon}_0} \right)^{0.02} = \frac{1}{\lambda_m} 0.0065 \max \left[1, 1 + \lambda_s \left(\frac{p}{f'_c} - \frac{1}{3} \right) \right] \left(\frac{\dot{\varepsilon}}{\dot{\varepsilon}_0} \right)^{0.02} \quad (7)$$

where ε_f is the failure strain of ceramic material, ε_m is the strain corresponding to the maximum compressive strength, λ_m is the shear damage at which strength reaches its maximum value under compression, and λ_s is an empirical constant.

The residual strength of the crushed ceramics is still high under the confining pressure. The residual strength surface for ceramic materials can be obtained from Eq.(4) by setting $f_t = 0$ and $f_{cc} = f'_c \times r$, namely

$$Y = \begin{cases} 3p \times r(\theta, e) & 0 < p \leq f'_c \times r/3 \\ \left[f'_c \times r + Bf'_c \tanh \left(\frac{p}{f'_c} - \frac{f'_c \times r}{3f'_c} \right) \right] \times r(\theta, e) & p > f'_c \times r/3 \end{cases} \quad (8)$$

where r is a constant, $f'_c \times r$ represents the residual strength of concrete under quasi-static uniaxial compression. Meanwhile, the initial yield strength of concrete under quasi-static uniaxial compression is defined as $f'_c \times l$.

2 Verification of the Newly-Developed Constitutive Model

The present model is verified against some available experimental data in terms of pressure-volumetric response, quasi-static strength surface and strain rate effect.

Values of various parameters in equation of state can be determined by hydrostatic compression experiment and they are listed in Table 1. For Al_2O_3 and SiC ceramic materials, the relationship between pressure and volumetric strain (Eq.(1)) can be rewritten as

$$p = 1.815 \times 10^{11} \mu + 1.208 \times 10^{12} \mu^2 - 2.991 \times 10^{12} \mu^3 \tag{9}$$

and, for AlN ceramic material, the relationship between pressure and volumetric strain (Eq.(2)) can be recast into the following form

$$p = \begin{cases} 1.815 \times 10^{11} \mu + 1.208 \times 10^{12} \mu^2 - 2.991 \times 10^{12} \mu^3 & \mu < 0.067 \\ 1.668 \times 10^{10} & 0.067 \leq \mu \leq 0.330 \\ 1.819 \times 10^{11} (\mu - 0.250) + 3.556 \times 10^{11} (\mu - 0.250)^2 - 2.830 \times 10^{11} (\mu - 0.250)^3 & \mu > 0.330 \end{cases} \tag{10}$$

Table 1 Values of parameters for BeO in the present model

Equation of state parameters				Constitutive model parameters			
K_1/GPa	K_2/GPa	K_3/GPa	$\rho_c/(\text{kg} \cdot \text{m}^{-3})$	F_m	W_x	W_y	S
181.5	1 207.9	-2 991	3 030	3	3.8	2	1.25
Constitutive model parameters							
f'_c/GPa	f_i/GPa	B	G/GPa	λ_m	λ_s	l	r
1.5	0.15	1.2	125	0.3	7.5	0.8	0.3

Fig.1 shows comparison of the present model predictions (Eq.(9) and Eq.(10)) with the experimental data for Al₂O₃ and SiC^[13-16] and for AlN^[17-19]. It can be seen from Fig.1 that good agreement is obtained.

Fig.2(a) and Fig.2(b) show comparisons between the present model predictions (Eq.(4) with $B = 1.4$ for B₄C and BeO and Eq.(9) with $B = 1.7$ for Al₂O₃ and AlN) and the test data^[25-27] for the strength surfaces. The strength surfaces of Al₂O₃ and AlN obtained from the JH-2 model^[28] are also shown in Fig.2(b). It is clear from Fig.2 that the present model predictions are in good agreement with available test results for ceramic materials. It is also clear from Fig.2(b) that the JH-2 model produces similar results to those of the present model for relatively low pressures whilst for higher pressure the present model levels out and the JH-2 model increases with increasing pressure.

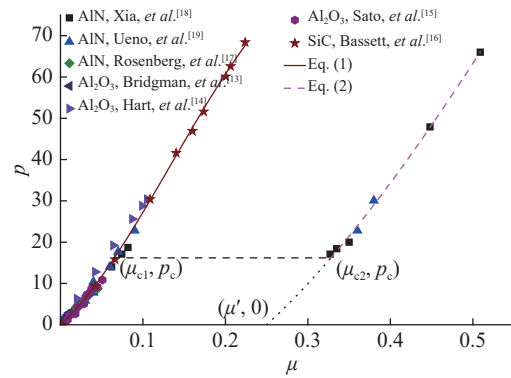
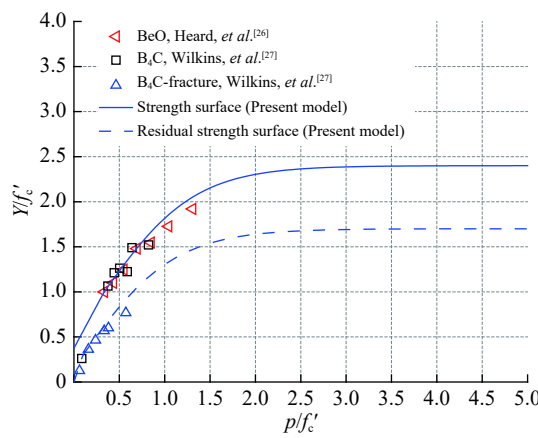
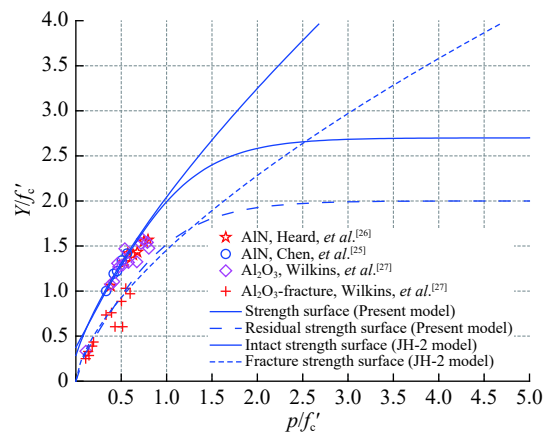


Fig. 1 Comparison between the present model predictions (Eq.(9) and Eq.(10)) and the experimental data for ceramic materials



(a) $B=1.4$ for B₄C and BeO



(b) $B=1.7$ for Al₂O₃ and AlN

Fig. 2 Comparisons between the present model predictions (Eq.(4) and Eq.(9)) with the experimental data

Values of parameters F_m , W_x and S in Eq.(6) for the dynamic increase factor in tension can be determined from tensile test data for ceramic materials at different strain rates. Fig.3 shows comparisons between the present model predictions (Eq.(6) with $F_m = 3$, $W_x = 3.8$ and $S = 1.25$) and available experimental data^[29-31] for different ceramic materials at different strain rates. It is evident from Fig.3 that reasonable agreement is obtained.

Fig.4(a) and Fig.4(b) show comparisons between the theoretically predicted strength surfaces (Eq.(4)) and some experimental data obtained from plate impact tests on B_4C ^[32-34], AlN ^[17], Al_2O_3 ^[20] and SiC ^[21-23]. In the calculations, a strain rate of $10^5 s^{-1}$ is taken which is of a typical value in a plate impact test. Also shown in Fig.4(b) are the predictions from the JH-2 model. It is clear from Fig.4(a) that reasonable agreement is obtained between the present model predictions and the tests results for B_4C which are somehow scattered whilst good agreement is achieved between Eq.(4) and the test data for AlN , Al_2O_3 and SiC as can be seen from Fig.4(b). It is also clear from Fig.4(b) that the JH-2 model has failed to predict the dynamic mechanical behavior of ceramic materials at higher confining pressure.

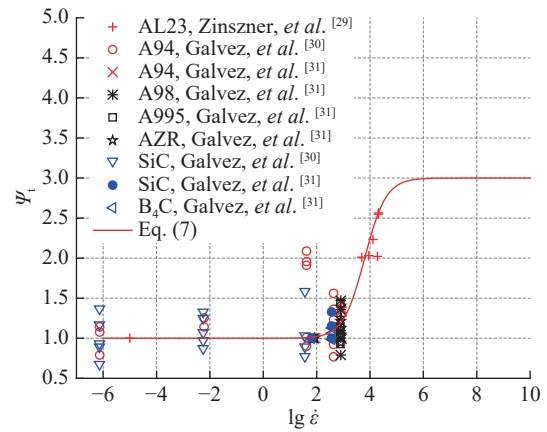


Fig. 3 Comparison between the present model predictions (Eq.(6)) with available experimental data for different ceramic materials at different strain rates (Unit of strain rate: s^{-1})

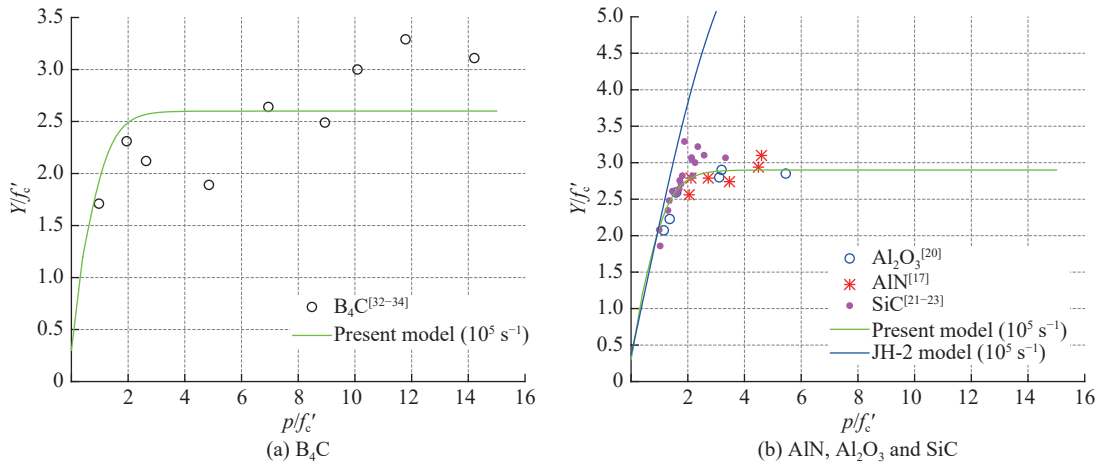


Fig. 4 Comparisons between the present model predictions (Eq.(4)) and the experimental data obtained from plate impact tests

Fig.5 shows comparison of the present model predictions and the experimental data obtained from SHPB (split Hopkinson pressure bar) tests^[25]. Also shown in the figure are the predictions from the JH-2 model. In the tests, confining pressures of up to 230 MPa were applied, and a constant strain rate was employed (i.e. $500 s^{-1}$). The solid line indicates theoretically predicted quasi-static strength surface, and the broken line designates dynamic strength surface from the present model with a strain rate of $500 s^{-1}$. As can be seen from Fig.5 that a good agreement is obtained between the present model predictions and the experimental data whilst the JH-2 model underestimates the strength surface of AlN ceramic under the strain rate of $500 s^{-1}$. It should be stressed here that the present model predicts that the quasi-static and dynamic strength surfaces are parallel to each other, which has been confirmed/verified by the experimental data. It leads to further support for the accuracy and validity of the present constitutive model for ceramics.

To demonstrate the quasi-static behavior of the present constitutive model, numerical tests are performed to evaluate stress-strain relationships for ceramics under various loading conditions, which includes: (a) triaxial compression with different confining pressures, (b) uniaxial tension, (c) biaxial tension and (d) triaxial tension. The numerical tests are carried out using single element simulation approach. Table 1 lists the values of various parameters in the present constitutive model for BeO ceramic. Table 2 and Table 3 list the values of various parameters for AlN ceramic employed in the present model and JH-2 model, respectively. Parameters in the present model are clearly defined in the previous paragraphs, and in JH-2 model. K_1, K_2, K_3 are bulk moduli, and ρ_c is the density for ceramic material; a, b, C, m, n are strength surface parameters; p_{HEL}, σ_{HEL} and μ_{HEL} are respectively the pressure, the equivalent stress and the volumetric strain at HEL (Hugoniot elastic limit); T is the maximum tensile hydrostatic pressure the material can withstand; β is strain rate parameter; d_1, d_2 are damage parameters.

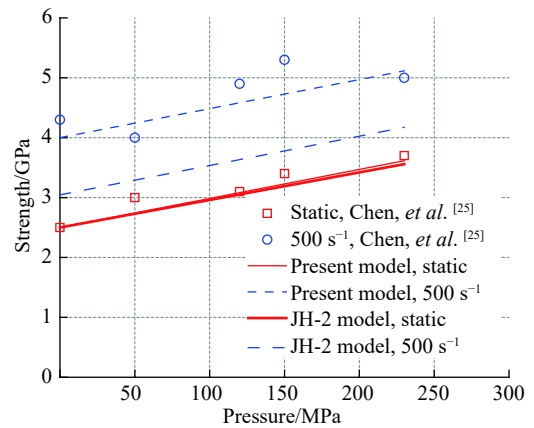


Fig. 5 Comparison between the experimental data^[25] and the predictions by the present model of strength varies with pressure at different strain rates of AlN

Table 2 Values of parameters for AlN in the present model

Equation of state parameters							Constitutive model parameters		
$\rho_c/(\text{kg}\cdot\text{m}^{-3})$	K_1/GPa	K_2/GPa	K_3/GPa	K_4/GPa	K_5/GPa	K_6/GPa	F_m	W_x	W_y
3 229	181.5	1 207.9	-2 991	181.9	335.6	-283	3	3.8	2
Constitutive model parameters									
f'_c/GPa	f_l/GPa	B	G/GPa	S	λ_m	λ_s	l	r	
3	0.3	1.7	127	1.25	0.3	7.5	0.8	0.3	

Table 3 Values of various parameters for AlN ceramic (JH-2 model)

Equation of state parameters				Constitutive model parameters					
$\rho_c/(\text{kg}\cdot\text{m}^{-3})$	K_1/GPa	K_2/GPa	K_3/GPa	a	b	C	n	m	
3 229	201	260	0	1.36	1.0	0.013	0.75	0.65	
Constitutive model parameters									
HEL/GPa	p_{HEL}/GPa	σ_{HEL}/GPa	μ_{HEL}	T/GPa	β	d_1	d_2		
9.0	5.0	6.0	0.024 2	0.32	1.0	0.02	1.85		

Fig.6 shows the comparison of the numerically predicted stress-strain curves and the experimental data for BeO under triaxial compression with confinement pressures ranging from 0.1 GPa up to 1.0 GPa, as reported by Heard and Cline^[26]. It is clear from Fig.6 that the numerical results are in reasonable agreement with the experimental observations.

Fig.7 shows variations of pressure and effective stress with maximum principal strain of AlN under quasi-static uniaxial tension. It is evident from Fig.7 that the numerical results from the present model give an elastic-brittle softening response of AlN under uniaxial tension with a principal tensile strength of 0.3 GPa for AlN. It is also evident from the figure that the mechanic behavior of the ceramic under uniaxial tension predicted

numerically by the JH-2 model is elastic-perfectly plastic with the minimum pressure of 0.31 GPa and the maximum effective stress of 0.93 GPa, which are obviously not in compliance with the actual tensile behavior of the ceramic.

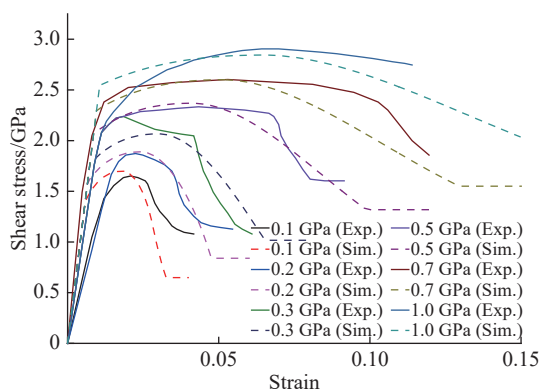


Fig. 6 Comparison of stress-strain curves for BeO under triaxial compression between the present model and experimental data^[22]

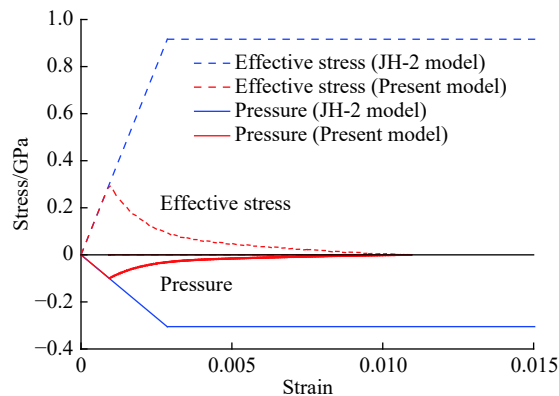


Fig. 7 Variation of pressure, effective stress with maximum principal strain for AlN under quasi-static uniaxial tension

Fig. 8 shows variations of pressure and effective stress with maximum principal strain of AlN under quasi-static biaxial tension. Elastic-brittle softening response of the ceramic is predicted numerically using the present model under biaxial tension with a principal tensile strength of 0.3 GPa. On the other hand, an elastic-perfectly plastic response of the ceramic under biaxial tension predicted numerically by the JH-2 model have the minimum pressure of 0.31 GPa and the maximum effective stress of 0.48 GPa.

Fig. 9 shows numerically predicted relationship between pressure and the maximum principal strain of AlN under both quasi-static triaxial tension. It can be seen from the figure that the present model predicts the elastic-brittle softening response of AlN under triaxial tension with quasi-static principal tensile strength of 0.3 GPa. Whilst the material is no longer able to withstand any loads after the maximum pressure reached according to the JH-2 model predictions. Furthermore, no strain rate effect is found under hydrostatic tension in the JH-2 model since it hasn't taken into account the strain rate effect in tension.

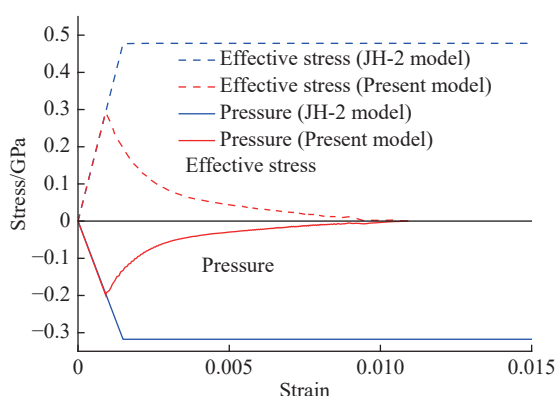


Fig. 8 Variation of pressure and effective stress with maximum principal strain for AlN under quasi-static biaxial tension

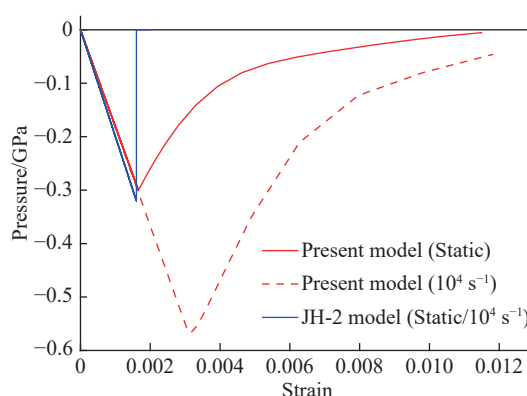


Fig. 9 Numerically predicted relationship between pressure and maximum principal strain of AlN under both quasi-static triaxial tension

3 Penetration of AD99.7/RHA Target

Numerical simulations are conducted in this section for the penetration of AD99.7/RHA target struck by flat-

nosed projectiles as reported by Lundberg^[35]. In the experiments, long tungsten projectiles with length-to-diameter ratio 15 were fired against the unconfined alumina with steel backing. The tests were carried out in three different scales with projectile lengths 30, 75 and 150 mm (corresponding diameters 2, 5 and 10 mm), respectively. The impact velocities were 1 500 m/s and 2 500 m/s. Fig. 10 shows the schematic diagrams of the geometric dimensions of the projectile-target combination. Table 4, Table 5 and Table 6 list the values of various parameters for AD99.7 ceramic material in the present model, tungsten alloy and RHA materials in the JC model. Parameters A_1 in the JC

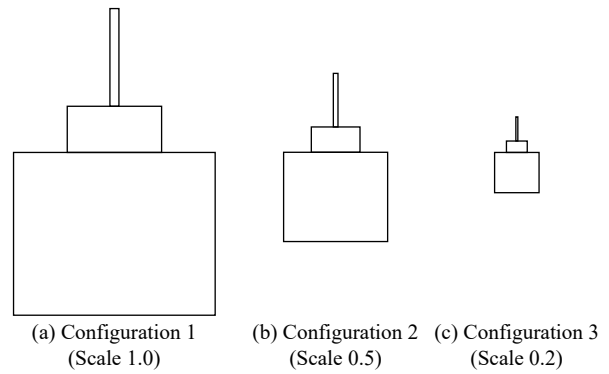


Fig. 10 Schematic diagrams of the geometric dimensions of the projectile-target combination under the impact velocity of 1 500 m/s (Same materials used for all target configurations, and all configuration are axisymmetric.)

model is the initial yield strength under reference strain rate and reference temperature; B_1, N_1 are respectively the strain hardening modulus and index; C_1 is strain rate hardening parameter; M_1 is temperature softening index; $\dot{\epsilon}_0$ is the reference strain rate; c_p is heat capacity; T_m and T_r are the ambient temperature and the reference temperature (melting point), respectively; D_1, D_2, D_3, D_4 and D_5 are failure criteria parameters; C_s is the intercept of shock wave velocity-particle velocity (u_s-u_p) curve; S_1, S_2, S_3 are u_s-u_p curve slope coefficient; γ_0 is Grüneisen parameter, A_0 is the first order volume correction of γ_0 .

Table 4 Values of various parameters for AD99.7 ceramic^[35] (The present model)

Equation of state parameters				Constitutive model parameters			
$\rho_0/(\text{kg}\cdot\text{m}^{-3})$	K_1/GPa	K_2/GPa	K_3/GPa	F_m	W_x	W_y	S
3 809	181.5	1 207.9	-2 991	3	3.8	2	1.25
Constitutive model parameters							
f'_c/GPa	f_t/GPa	B	G/GPa	λ_m	λ_s	l	r
3	0.3	1.4	135	0.3	7.5	0.8	0.3

Table 5 Values of various parameters for tungsten alloy^[35] (JC model)

Constitutive model parameters							
$\rho_0/(\text{kg}\cdot\text{m}^{-3})$	G/GPa	A_1/GPa	B_1/GPa	N_1	C_1	M_1	$\dot{\epsilon}_0/\text{s}^{-1}$
17 600	122	1.506	0.177	0.12	0.016	1.0	1.0
Constitutive model parameters							
$c_p/(\text{J}\cdot\text{kg}^{-1}\cdot\text{K}^{-1})$	T_m/K	T_r/K	D_1	D_2	D_3	D_4	D_5
134	1 723	300	2.0	0	0	0	0
Equation of state parameters							
$C_s/(\text{m}\cdot\text{s}^{-1})$	S_1	S_2	S_3	γ_0	A_0		
4 029	1.23	0	0	1.54	0.4		

Fig. 11 shows the comparison of total penetration depth between the numerical predictions and the experimental data^[35]. P_T represents the sum of thickness of the ceramic and penetration depth in the RHA back plate, and L_p is the length of the projectile. In the figure, the solid symbols indicate the experimental data and the hollow symbols represent the numerical results by the present model proposed in this paper. The data of different

Table 6 Values of various parameters for RHA^[35] (JC model)

Constitutive model parameters							
$\rho_0/(\text{kg}\cdot\text{m}^{-3})$	G/GPa	A_1/GPa	B_1/GPa	N_1	C_1	M_1	$\dot{\epsilon}_0/\text{s}^{-1}$
7 800	77	0.792	0.51	0.26	0.014	1.03	1.0
Constitutive model parameters							
$c_p/(\text{J}\cdot\text{kg}^{-1}\cdot\text{K}^{-1})$	T_m/K	T_l/K	D_1	D_2	D_3	D_4	D_5
477	1 793	294	0.05	3.44	-2.12	0.002	0.61
Equation of state parameters							
$C_s/(\text{m}\cdot\text{s}^{-1})$	S_1	S_2	S_3	γ_0	A_0		
4 569	1.49	0	0	2.17	0.460		

scales under the impact velocity of 1 500 m/s and 2 500 m/s are designated by square and triangle, respectively. For comparison, the numerical results obtained by Lundberg^[35] with JH-2 model are also shown in Fig.11. The solid and broken lines represent the numerical results by JH-2 model at 1 500 m/s and 2 500 m/s respectively. It can be seen from Fig.11 that the numerical results from the present model are in good agreement with the experimental data. As can be seen from the figure that the numerical results for impact velocity of 1 500 m/s are in good agreement with the test data, whilst the results for impact velocity of 2 500 m/s are below the experimental observations^[35].

Thus, the JH-2 model has failed to produce consistent results as compared to the experiments.

4 Conclusions

A dynamic macroscopic constitutive model for ceramic materials has been developed by closely following the previous work on concrete. The model captures the basic features of the mechanical response of ceramic materials including pressure hardening behavior, strain rate effects, strain softening behavior, path dependent behavior (Lode angle), and failure in both low and high confining pressures. In particular, a new function is used to characterize the pressure dependent shear strength surface of ceramic materials which levels out at very high pressures, and strain rate effect is taken into consideration by dynamic increase factor which excludes inertial effect.

The present model has been compared with some available experimental data for ceramic materials. It transpires that the present model predictions are in good agreement with the experimental observations in terms of pressure-volumetric response, triaxial compression, quasi-static strength surface, dynamic strength surface, strain rate effect and depth of penetration. It also transpires that the present model is much more improved than the JH-2 model.

References:

- [1] FAHRENTHOLD E P. A continuum damage model for fracture of brittle solids under dynamic loading [J]. *Journal of Applied*

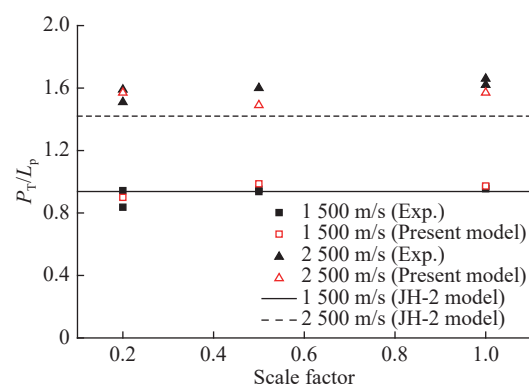


Fig. 11 Comparison between the numerical results and the test data for the depth of penetration in AD99.7/RHA targets by flat-nosed tungsten alloy penetrators^[35]

- Mechanics*, 1991, 58(4): 904–909.
- [2] RAJENDRAN A M. Modeling the impact behavior of AD85 ceramic under multiaxial loading [J]. *International Journal of Impact Engineering*, 1994, 15(6): 749–768.
- [3] JOHNSON G R, HOLMQUIST T J. An improved computational constitutive model for brittle materials [J]. *High Pressure Science and Technology*, 2008, 309(1): 981–984.
- [4] SIMHA C H, BLESS S, BEDFORD A, et al. Computational modeling of the penetration response of a high-purity ceramic [J]. *International Journal of Impact Engineering*, 2002, 27(1): 65–86.
- [5] RAVICHANDRAN G, SUBHASH G. A micromechanical model for high strain rate behavior of ceramics [J]. *International Journal of Solids and Structures*, 1995: 2627–2646.
- [6] ESPINOSA H D. On the dynamic shear resistance of ceramic composites and its dependence on applied multiaxial deformation [J]. *International Journal of Solids and Structures*, 1995, 32(21): 3105–3128.
- [7] ESPINOSA H D, XU Y, BRAR N S. Micromechanics of failure waves in glass: II, modeling [J]. *Journal of the American Ceramic Society*, 1997, 80(8): 2074–2085.
- [8] STEINBERG D J. Computer studies of the dynamic strength of ceramics [M]//*Shock Waves*. Berlin: Springer, 1992: 415–422.
- [9] XU H, WEN H M. A computational constitutive model for concrete subjected to dynamic loadings [J]. *International Journal of Impact Engineering*, 2016, 91: 116–125.
- [10] XU H, WEN H M. Semi-empirical equations for the dynamic strength enhancement of concrete-like materials [J]. *International Journal of Impact Engineering*, 2013, 60: 76–81.
- [11] ZHAO F Q, WEN H M. A comment on the maximum dynamic tensile strength of a concrete-like material [J]. *International Journal of Impact Engineering*, 2018, 115: 32–35.
- [12] ZHAO F Q, WEN H M. Effect of free water content on the penetration of concrete [J]. *International Journal of Impact Engineering*, 2018, 121: 180–190.
- [13] BRIDGMAN P W. Linear compressions to 30 000 kg/cm², including relatively incompressible substances [J]. *Proceedings of the American Academy of Arts and Sciences*, 1949, 77(6): 189–234.
- [14] HART H V, DRICKAMER H G. Effect of high pressure on the lattice parameters of Al₂O₃ [J]. *Journal of Chemical Physics*, 1965, 43(7): 2265–2266.
- [15] SATO Y, AKIMOTO S. Hydrostatic compression of four corundum-type compounds: α -Al₂O₃, V₂O₃, Cr₂O₃, and α -Fe₂O [J]. *Journal of Applied Physics*, 1979, 50(8): 5285–5291.
- [16] BASSETT W A, WEATHERS M S, WU T C, et al. Compressibility of SiC up to 68.4 GPa [J]. *Journal of Applied Physics*, 1993, 74(6): 3824–3826.
- [17] ROSENBERG Z, BRAR N S, BLESS S J. Dynamic high-pressure properties of AlN ceramic as determined by flyer plate impact [J]. *Journal of Applied Physics*, 1991, 70(1): 167–171.
- [18] XIA Q, XIA H, RUOFF A L. Pressure induced rocksalt phase of aluminum nitride: a metastable structure at ambient condition [J]. *Journal of Applied Physics*, 1993, 73(12): 8198–8200.
- [19] UENO M, ONODERA A, SHIMOMURA O, et al. X-ray observation of the structural phase transition of aluminum nitride under high pressure [J]. *Physical Review B*, 1992, 45(17): 10123.
- [20] ROSENBERG Z, YAZIV D, YESHURUN Y, et al. Shear strength of shock-loaded alumina as determined with longitudinal and transverse manganin gauges [J]. *Journal of Applied Physics*, 1987, 62(3): 1120–1122.
- [21] BOURNE N K, MILLETT J, PICKUP I, et al. Delayed failure in shocked silicon carbide [J]. *Journal of Applied Physics*, 1997, 81(9): 6019–6023.
- [22] FENG R, RAISER G F, GUPTA Y M, et al. Material strength and inelastic deformation of silicon carbide under shock wave compression [J]. *Journal of Applied Physics*, 1998, 83(1): 79–86.
- [23] PICKUP I M, BARKER A K. Deviatoric strength of silicon carbide subject to shock [J]. *AIP Conference Proceedings*, 2000, 505(1): 573–576.
- [24] LEE M, BRANNON R M, BRONOWSKI D R. Uniaxial and triaxial compression tests of silicon carbide ceramics under quasi-static loading condition [R]. Albuquerque, New Mexico: Sandia National Laboratories, 2005.
- [25] CHEN W, RAVICHANDRAN G. Static and dynamic compressive behavior of aluminum nitride under moderate confinement [J]. *Journal of the American Ceramic Society*, 1996, 79(3): 579–584.

- [26] HEARD H C, CLINE C F. Mechanical behaviour of polycrystalline BeO, Al₂O₃ and AlN at high pressure [J]. *Journal of Materials Science*, 1980, 15(8): 1889–1897.
- [27] WILKINS M L, CLINE C F, HONODEL C A. Fourth progress report of light armor program [R]. Livermore: Lawrence Radiation Laboratories, 1969.
- [28] HOLMQUIST T J, TEMPLETON D W, BISHNOI K D. Constitutive modeling of aluminum nitride for large strain, high-strain rate, and high-pressure applications [J]. *International Journal of Impact Engineering*, 2001, 25(3): 211–231.
- [29] ZINSZNER J L, ERZAR B, FORQUIN P, et al. Dynamic fragmentation of an alumina ceramic subjected to shockless spalling: an experimental and numerical study [J]. *Journal of the Mechanics and Physics of Solid*, 2015, 85: 112–127.
- [30] GALVEZ F, RODRIGUEZ J, SANCHEZ V. Tensile strength measurements of ceramic materials at high rates of strain [J]. *Le Journal de Physique IV*, 1997, 7(C3): 151.
- [31] GALVEZ F, RODRIGUEZ J, SANCHEZ V. The spalling of long bars as a reliable method of measuring the dynamic tensile strength of ceramics [J]. *International Journal of Impact Engineering*, 2002, 27(2): 161–177.
- [32] BOURNE N K. Shock-induced brittle failure of boron carbide [J]. *Proceedings of the Royal Society of London. Series A: Mathematical, Physical and Engineering Sciences*, 2002, 458: 1999–2006.
- [33] VOGLER T J, REINHART W D, CHHABILDAS L C. Dynamic behavior of boron carbide [J]. *Journal of Applied Physics*, 2004, 95: 4173–4183.
- [34] HAYUN S, PARIS V, DARIEL M P, et al. Static and dynamic mechanical properties of boron carbide processed by spark plasma sintering [J]. *Journal of the European Ceramic Society*, 2009, 29(16): 3395–3400.
- [35] LUNDBERG P, WESTERLING L, LUNDBERG B. Influence of scale on the penetration of tungsten rods into steel-backed alumina targets [J]. *International Journal of Impact Engineering*, 1996, 18(4): 403–416.

陶瓷材料宏观动态新本构模型

唐瑞涛, 徐柳云, 文鹤鸣, 王子豪

(中国科学技术大学材料力学行为和设计重点实验室, 安徽 合肥 230027)

摘要: 基于已有混凝土材料的相关研究, 建立了陶瓷材料在动态载荷作用下的宏观本构模型。模型中状态方程采用多项式描述, 强度面模型中考虑了压力相关性、Lode角效应、应变率效应、剪切损伤及拉伸软化等的影响。采用一个新的函数来描述陶瓷材料的强度面, 其在较高压力下趋于一个平台值; 并采用动态增强因子 (DIF) 考察剥除惯性效应后陶瓷材料的真实应变率效应。通过将模型预测的压力-体应变响应、准静态强度面以及应变率效应与相关实验数据进行对比, 验证了该模型。单个单元测试模拟得到的结果与三轴实验数据以及侵彻实验数据高度吻合, 进一步验证了此模型。为显示模型的优越性, 还与 JH-2 模型的预测结果进行了比较。结果表明: 所提出的本构模型能够很好地预测陶瓷材料在不同加载条件下的力学行为, 且优于现有的模型。

关键词: 陶瓷材料; 本构模型; 应变率效应; 三轴实验; JH-2 模型; 单单元测试

中图分类号: O347.3

文献标识码: A